Beam Thermal Blooming
Turbulence
- Winds Atmospheres ep

Effect of a random wind field on thermal blooming instabilities

J. R. Morris, J. A. Viecelli, and T. Karr

Lawrence Livermore National Laboratory, Livermore, CA 94550

ABSTRACT

We have numerically investigated the effect of random fluctuations on uncompensated (open-loop) and phase-compensated (closed-loop) small-scale thermal blooming instabilities of a collimated beam propagating through refractive index turbulence. We used the ORACLE time-dependent, three space-dimensional, wave-optics code on a Cray X-MP. The Monte Carlo random wind fields, v(z), were exponentially correlated along the propagation direction, z. The small scale instabilities are present up to a threshold value of the rms random wind, beyond which beam propagation appears to be stable; the threshold value is nearly independent of the correlation length as long as the latter is much shorter than both the length of the thermal blooming region and the Rayleigh range of dominant perturbations. We describe our results with a dimensionless shear parameter, S, that is directly proportional to the ratio of the turbulence scintillation rate to the thermal blooming rate. S is defined as: $S=(\sigma_v/\dot{N}_\lambda)\cdot\sqrt{3\pi/(\lambda L)}$ where σ_v is the one-axis variance of the random wind and $\dot{N}_\lambda$ is the time derivative of the thermal blooming optical path difference (OPD) in waves/sec.

The open-loop calculations use a plane wave "beam" and a uniform medium. The Strehl ratio at 50 waves of thermal blooming OPD remains approximately constant while $S \geq 2.3$ and then it decreases rapidly as S decreases.

The closed-loop calculations use a large Fresnel number finite beam, a non-uniform medium of length 2L, absorption $\propto \exp(-z/L)$, and a Hufnagel-Valley type C_N^2 profile whose r_0 Fresnel number was 24. For $10 \leq N_p \leq 40$ we see no evidence of the closed-loop instability at a wind clearing time (20 waves) for $S \geq (54 \pm 2)/N_p$, where $N_p = \pi\Lambda_p^2/4\lambda L$ and Λ_p is twice the actuator spacing simulated by a Fourier filter. This result suggests that the ratio of the turbulence scintillation rate to the closed-loop gain for a uniform wind determines the threshold.

1. INTRODUCTION

Prior to late 1986 the high-power laser research community in the United States believed that whole beam blooming effects[1] would determine the maximum tolerable thermal blooming optical path difference (OPD) that is consistent with a high Strehl ratio propagation of phase-compensated, collimated beams over paths with very large Fresnel numbers. This whole beam OPD limit is directly proportional to the whole beam Fresnel number, leading to a P/D^3 scaling law, where P is the laser power and D is its beam diameter. The only recognized uncertainty was the correctability of the turbulence thermal-blooming interaction[2] which was defined at that time to be thermal blooming caused by turbulence speckle when the sources of both were far from the transmitting aperture.

More recent calculations and theoretical work at Livermore,[3-5] has shown that such propagation of collimated, very large Fresnel number beams is unstable to small scale perturbations this also has been noted by workers at Lincoln Laboratory,[6] and Northeast Research Associates[7]. Furthermore, these groups found that growth of small-scale phase and intensity inhomogeneities will determine the maximum tolerable thermal blooming OPD, especially in the presence of a realistic level of turbulence. For the unidirectional wind plus beam slewing velocity field model used in the both the calculations and the theory the thermal blooming OPD limit set by these small-scale instabilities is independent of the beam diameter; this leaves the P/D scaling of the OPD itself. However, the simple wind model left open the question, "Does the variation of wind direction along the propagation path – caused by large scale eddies associated with velocity turbulence – significantly alter the results?" The answer is yes, as we shall show in this paper.

Figure 1 describes the instability growth processes, the inhomogeneity sources that seed instabilities, and the damping mechanisms that reduce or suppress the instability growth. Net perturbation growth is the result of competition between the growth and damping mechanisms. The coupling that causes growth is described by the cycle: (1) ray bending or diffraction converts phase perturbations into irradiance perturbations, (2) irradiance perturbations write refractive index perturbations into the propagation medium via absorption, and (3) propagation through the refractive index perturbations creates phase perturbations. While this cycle does not preclude local modes, steps (1) and (3) strongly favor axial coherence over a large portion of the thermal blooming layer. Processes that reduce axial coherence are damping mechanisms that reduce instability growth rates.

The wavenumbers for which perturbation growth can be important ranges from a few times $2\pi/D$ up to the point at which diffusion damping exceeds the perturbation growth rate. The low end of this range, up to about $2\pi/r_0$ where r_0 is Fried's coherence length for turbulence, must be corrected by the phase compensation system to achieve satisfactory

correction for turbulence. Within this correction pass-band perturbations grow by a process that is now known as the closed-loop[4] or phase compensation instability (PCI). At wavenumbers above the pass-band the open-loop instability, also known as Stimulated Thermal Rayleigh Scattering[8] (STRS), causes perturbations to grow. A significant, perhaps the dominant, source is refractive index turbulence, which is present over the entire range of wavenumbers. Within the compensated wavenumber range irradiance and phase irregularities on the beam at the transmitting aperture (called noise in Fig. 1) are also sources. Other sources above the compensated range include the fitting error inherent in real wavefront-sensor/deformable-mirror systems and nonlinear mixing of the perturbations being generated with wavevectors inside the correction pass-band.

The damping mechanisms include molecular diffusion at size scales of centimeters or millimeters, local velocity variations at size scales up to the beam diameter (turbulent mixing), and velocity variations at size scales much larger than the beam diameter up to the entire propagation path length. The size scales of the latter are large enough that a good first approximation is a velocity field that varies along the propagation distance coordinate, but not along the orthogonal transverse coordinates. These velocity changes damp the growth of a sinusoidal intensity perturbation by transporting the heat across its peaks and valleys, thereby reducing the OPD change that would cause it to grow. The magnitude and especially the direction changes in the wind velocity along the propagation path reduce the axial coherence by shifting the sinusoidal refractive index profiles of the Fourier modes relative to the phase and irradiance profiles, thereby reducing the OPD that the beacon and high-power laser accumulate.

When the instability growth equations are written in terms of dimensionless variables[9], the magnitude of the axial variation of the wind velocity is naturally characterized by a dimensionless parameter, S, which is directly proportional to the ratio of perturbation scrambling to the blooming rate:

$$S = \sqrt{\frac{\pi}{4\lambda L}}\,\frac{\Delta v}{\dot{N}_\lambda} \qquad (1)$$

where Δv for various velocity field models is given in Table 1, L is the thickness of the thermal blooming layer, and $\dot{N}_\lambda$ is the time derivative of the thermal blooming optical path difference (OPD) in waves/sec. In the dimensionless equations the transverse size scale of the perturbations is measured by a Fresnel number

$$N_p = \frac{\pi}{4}\frac{\Lambda_p^2}{\lambda L} \qquad (2)$$

with $\Lambda_p = 2\pi/(\text{perturbation wave number})$.

Table 1. Definitions of Δv for slewed beams and random winds.

Phenomenon	Δv
Slewing (linear shear)	ΩL (= $\|v(L) - v(0)\|$) for uniform wind
Random winds	$\sqrt{12}\sigma_v$ (1-axis)

Fig. 2 shows perturbation growth rate dispersion curves for wavevectors parallel to the slewing direction for slewed laser beams with various dimensionless slew rates, S. (The smooth curves are a WKB theory and the circles are results obtained with our nonlinear wave-optics propagation code, ORACLE.) As the slewing rate is increased from zero, first the growth rate for large wavenumber (small N_p) perturbations is reduced, then growth at all wavenumbers is reduced. Finally, for $S > 5$ exponential growth of perturbations ceases at all wavenumbers, Unfortunately, as was first recognized by Rosenbluth[10], suppression of perturbation growth by linear shear (slewing) is anisotropic. It is described by a dimensionless shear which is directly proportional to $\Delta \mathbf{v} \cdot \hat{\mathbf{k}}_\perp$, so that $S = 0$ for wavevectors that are orthogonal to the slewing direction; i.e., the perturbation growth rate for these wavevectors is unchanged by the slewing. Nevertheless, from the slewed beam results, wind fields in which Δv varies significantly in direction as well as magnitude over path segments small compared to the blooming layer thickness, L, were expected to significantly reduce growth or to eliminate it altogether at some critical S value.

To characterize the magnitude of the dimensionless shear S that eliminates or substantially reduces growth we have performed numerical simulations performed with our ORACLE wave-optics propagation code for a wind field consisting of a uniform plus a random component. The random velocity component is generated by a transversely isotropic vector Markov process[11] such that its ensemble has zero mean and a specified one-axis rms value. For a constant propagation step, Δz, given the velocity at z, the velocity at $z+\Delta z$ is calculated by

$$v(z+\Delta z) = v(z) \cdot \exp(-\Delta z/Z_c) + (a_x, a_y) \qquad (3)$$

where $a_{x,y}$ are both zero-mean statistically independent Gaussian random variables whose variance is

$$\langle a_{x,y}^2 \rangle = 2\sigma_v[1 - \exp(-\Delta z/Z_c)] \qquad (4)$$

and Z_c is the correlation length for the Markov velocity field.

2. OPEN-LOOP RESULTS

Even in compensated systems there will be a substantial range of wavevectors which lie above the correction regime. For these wavevectors perturbation growth is open-loop because the correction system is incapable of sensing or applying phase compensation at these small transverse spatial scales. In our computational study of the effect of random wind fields on the open-loop instability growth rate we used so called "patch beam" simulations in which the unperturbed field fills the computational mesh; i.e., it is a sample of an infinite plane wave. We used a z-independent absorption coefficient and constant laser wavelength, pathlength, velocity variance and turbulence coherence length. The strength of the turbulence is as $N_T = \pi/4$, where the turbulence Fresnel number is defined to be $N_T = \pi r_0^2/4\lambda L$. For the cases presented here the correlation length of the Markov velocity field was 18% of the propagation path length; computations using a correlation length 1.8% of the propagation path length gave nearly identical results. We varied the dimensionless shear, S, by changing the rate of accumulation of thermal blooming OPD, $\dot{N}_\lambda$. Our calculations usually employed 250 propagation steps and a 32 X 32 transverse mesh; excursions to 64 X 64 X 1000 assured us that this spatial resolution was sufficient. Our time step provided at least 6.8 samples per scintillation autocorrelation time and at least 6 samples per wave of thermal blooming OPD.

Figure 3 gives the "Strehl ratio" [(Power at k = 0) / (total power)] as a function of the dimensionless shear parameter, S, after 50 waves of thermal blooming OPD. For shear S > 2.3 the Strehl ratio is near that due to turbulence alone(S = ∞); near S = 2.3 there is a sharp threshold where a small decrease in S leads to a large decrease in the Strehl ratio. Figure 4 illustrates the difference between the temporal evolution of the Strehl ratio above and below the stability threshold S = 2.3; in the stable region S > 2.3 (solid curve) it oscillates with a slowly decreasing envelope corresponding to at most an algebraic growth of the perturbations. Below S = 2.3 (dotted curve) the envelope falls steeply corresponding to quasi-exponential growth of perturbations, such as is analytically predicted for the S = 0 case.

3. CLOSED LOOP RESULTS

To study the effect of a random wind field on propagation of a phase-compensated beam we used a finite beam for which the thermal blooming rate was 10 waves/sec and the clearing time set by the non-random uniform component of the wind was 2 sec. The intensity profile was an $\exp[-r^{20}]$ approximation to a uniformly illuminated circular aperture. The absorption profile was exp[-2z/L] and the C_N^2 turbulence profile was proportional to a Hufnagel-Valley profile[12] at 0.5 μm with r_0 = 5 cm, θ_0 = 7μrad, and 2 km altitude scaled to an absorption e-fold. At the 1 μm laser wavelength this profile had a turbulence Fresnel number of about 23. The correction system's finite spatial resolution was modeled by a $2^{-(k/k_{1/2})^{20}}$ Fourier filter. Figure 5 shows the Strehl ratio versus

time for various dimensionless shear values, S. The Fresnel number of perturbations at the phase compensation roll-off $k = k_{1/2}$ was $N_p = 10$. For $S < 3$ the characteristic behavior associated with a large PCI growth rate is clearly evident; the Strehl ratio remains high for a few waves of blooming and then suddenly plunges to a low value. At larger values of S the Strehl ratio cliff occurs at larger thermal blooming OPD values until somewhere in the interval $5.2 \leq S \leq 6.9$ no signature of PCI growth is present. Figure 6 illustrates the typical path end (near field) intensity profile for a case with no PCI signature (S = 5.60) and a case with a noticeable PCI signature (S = 4.3). The S = 5.60 case has an intensity profile nearly identical to that caused by turbulence alone while the S = 4.3 case shows pronounced bright and dark areas in the down wind portion of the beam. Furthermore, the spatial separation between bright areas is approximately equal to, but slightly longer than, $2\pi/k_{1/2}$, as is expected for PCI.

We also examined $N_p = 13.3$, 20 and 40. The behavior of the Strehl versus time curves for $N_p = 13.3$ and 20 are qualitatively similar to those for $N_p = 10$, with a clear transition between PCI and no PCI signature (the Strehl step). The $N_p = 40$ case shown in Fig. 7 has a more ambiguous signature of instability onset. We believe that the transition near 0.1 sec from a small slope for S = 1.29 to a much steeper slope for S = 0.86 is a signature of unsuppressed open-loop (STRS) growth and that the PCI gain ($\propto 1/N_p$) is simply too small for any evidence of it to be seen in these curves.

Figure 8 shows the boundary between instability and apparent stability. The upper set of vertical bars is the pure phase-compensation results. At S values above the top of these bars we see no signature of instability, either open- or closed-loop. Below the bottom of these bars we see clear evidence of PCI for $N_p = 10$, 13.3, and 20; and a suggestion of STRS for $N_p = 40$. A straight line $S = 54/N_p$ is a good fit to this data. (While our Strehl ratio results for a finite beam show apparent stability above these S values, there may actually be algebraic or even very slow exponential growth that is simply not apparent by 20 waves of thermal blooming OPD.)

In addition we have explored instability growth for simultaneous intensity and phase compensation. Finite resolution of intensity compensation was modeled with a Fourier filter that was identical to the filter used for the phase-compensation in each case. The results are the lower set of vertical bars in Figure 8. Intensity compensation yields stable behavior for dimensionless shears about 0.3 times those required for stable behavior for phase-only compensation.

4. SUMMARY

We have investigated the effect of a transversely isotropic Markov wind field on PCI and STRS growth rates when the Markov correlation length is much less then the thermal blooming layer thickness. We found that $S \geq 2.3$ suppresses quasi-exponential STRS

growth out to 100 or more waves of blooming; in terms of absorbed power, $\alpha L I_0$, in W/cm^2 this limit is

$$\alpha L I_0 \leq 3.9 \sigma_v \quad (5)$$

where σ_v is in m/s. For $40 \geq N_p \geq 10$ we also found that $S \geq 56/N_p$ suppresses all evidence of exponential PCI growth in Strehl ratio versus time plots out to at least 20 waves blooming; the corresponding absorbed power limit is

$$\alpha L I_0 \leq 0.16 N_p \sigma_v. \quad (6)$$

Assuming that these threshold S values represent true suppression of exponential growth, as is the case for STRS, the boundary between high Strehl ratio and low Strehl ratio propagation will scale like $\dot{N}_\lambda \propto P/D^2$.

Intensity and phase compensation with identical transverse correction scales raises the above absorbed power limits (lowers the required dimensionless shear) by a factor of about 3.2

5. ACKNOWLEDGEMENTS

Work performed under the auspices of the U.S. Department of Energy by Lawrence Livermore National Laboratory under contract W-7405-ENG-48 for the U.S. Army in support of MIPR No. W31RPD-7-D4041.

6. REFERENCES

1. J. Herrmann, "Properties of phase conjugate adaptive optical systems," J. Opt. Soc. Am. 67, 290-295, (1977).

2. J. Herrmann, (private communication, 1985).

3. R. J. Briggs, "Models of high spatial frequency thermal biooming instabilities," Lawrence Livermore National Laboratory Report, UCID-21118 (14 August 1987).

4. T. J. Karr, "Thermal blooming compensation instabilities," J. Opt. Soc. Am. A 6, 1038-1048 (1989).

5. J. R. Morris, "Scalar Green's function derivation of the thermal blooming compensation instability equations," to be published in JOSA A 6 (December 1989). Also, Lawrence Livemore National Laboratory Report, UCID-21261 (14 October 1987)

6. J. Schonfeld, (private communications, 1988-1989); H. Praddaude, (private communications, 1987-1988)

7. B. Myers, (private communications, 1987-1989); B. Hatfield, (private communications, 1988-1989)

8. See for example, W. Kaiser and M. Maier, "Stimulated Rayleigh, Brillouin, and Raman Spectroscopy," in Laser Handbook, vol. 2, F. T. Arecchi and E. O. Shulz-Dubois, eds., pp. 1077-1150 (North Holland, Oxford, 1972) and references therein. Also, H. J. Hoffman, "Thermally induced phase conjugation by transient real-time holography: a review," J. Opt. Soc. Am. B 3, 253-273 (1986) and references therein.

9. The dimensionless coordinates are: z/L (axial), $(x,y)/\sqrt{\lambda L}$ (transverse), and $\dot{N}_\lambda t$ (temporal) where $\dot{N}_\lambda$ is the time rate-of-change of the thermal blooming OPD (in waves) for zero wind velocity.

10. M. Rosenbluth, (private communication, 1987).

11. J. A. Viecelli, "Thermal blooming threshold computations with a Markov model of velocity turbulence," Lawrence Livermore National Laboratory Report, UCID-21589 (30 November 1988).

12. P. B. Ulrich, "Huffnagel-Valley profiles for specified values of the coherence length and isoplanatic patch angle," W. J. Shafer Associates, Inc. Report, WJSA/MA/TN-88-013 (27 April 1988).

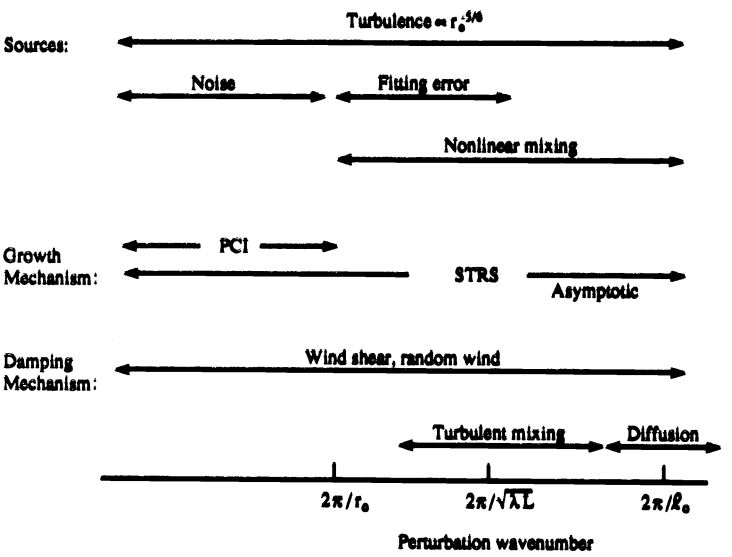

Fig. 1. Thermal blooming instability phenomena in wavenumber space.

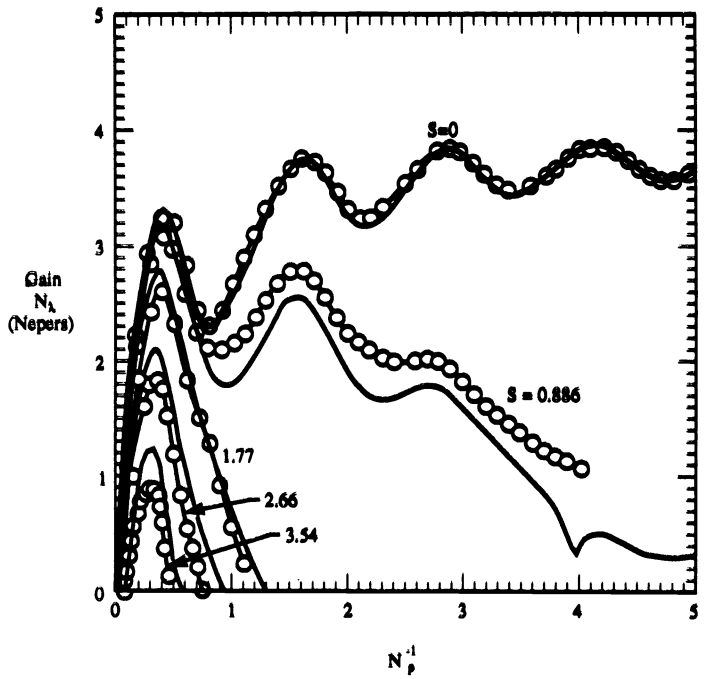

Fig. 2. Closed-loop instability dispersion curves for various linear wind shear values, S. The abscissa, N_p^{-1}, is directly proportional to the propagation path length normalized to a perturbation diffraction length. All results are for a uniform absorption coefficient, a velocity field that is a linear function of the propagation distance (linear shear), and spatially exact, temporally instantaneous phase-only compensation. The curves are WKB theory analytic results; the circles are values obtained from the ORACLE nonlinear wave-optics code.

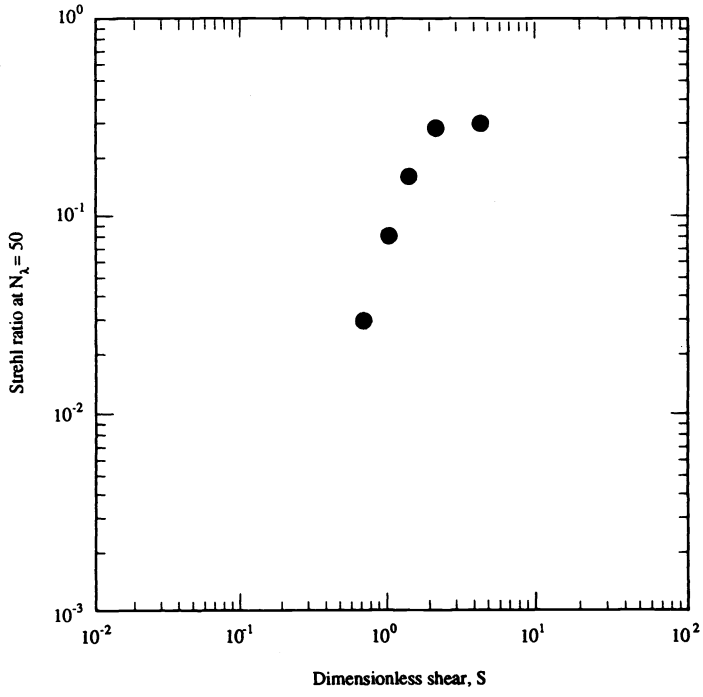

Fig. 3. Strehl ratio of an uncompensated plane wave propagating through turbulence as a function of the dimensionless shear value, S. The results are at 50 waves of thermal blooming OPD. The correlation length of the Markov velocity field was 18% of the propagation path length and the turbulence Fresnel number $\left(\pi r_0^2/4\pi L\right)$ was $\pi/4$. The absorption coefficient and turbulence structure constant were constant along the propagation path. The periodic patch width was $\sqrt{10}r_0$ and the "patch-beam Strehl ratio" corresponds to a tilt compensated Strehl ratio for the patch size.

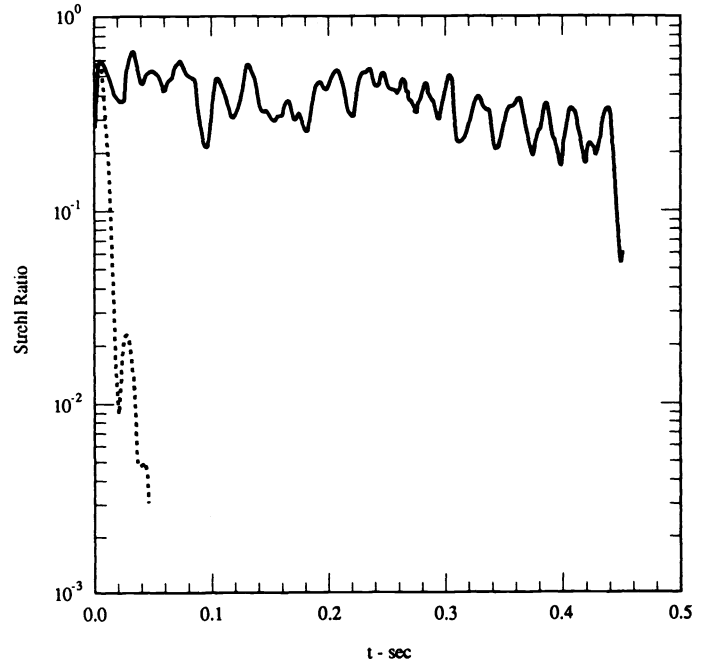

Fig. 4. Time dependence of the Strehl ratio for the stable (solid curve) and unstable cases (dotted curve). At the end of the solid curve about 132 waves of thermal blooming OPD have accumulated.

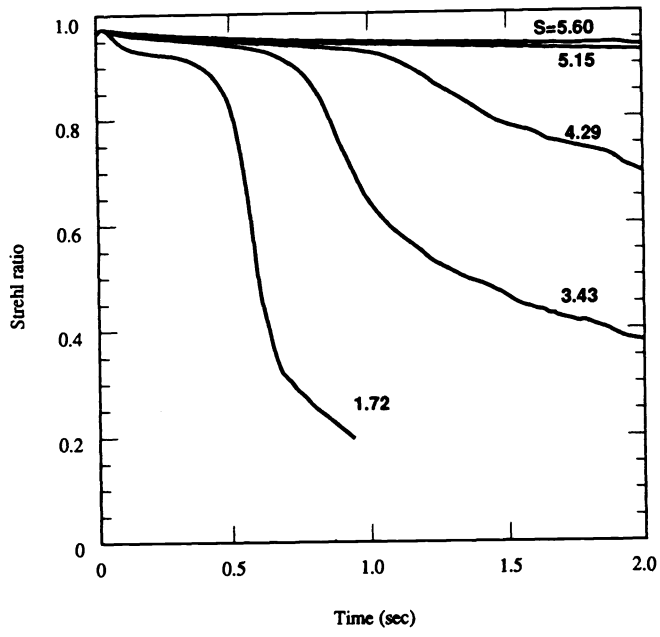

Fig. 5. Phase-compensated Strehl ratio versus time curves for a perturbation Fresnel number $N_p = 10$ and various shear values, S. The thermal blooming rate is 10 waves/s and the laser intensity is an $\exp(-r^{20})$ approximation to a uniformly illuminated circular aperture.

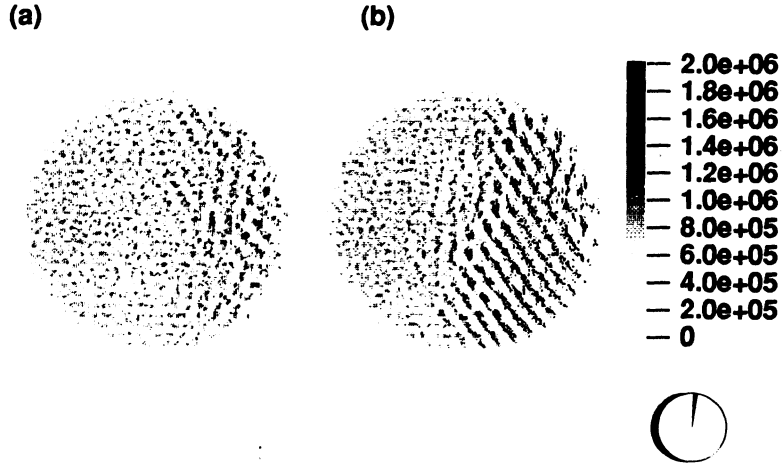

Fig. 6. Typical near-field intensity profiles of the high-power beam at the end of the propagation path for $N_p = 10$: (a) S = 5.60 where no instability growth is evident, (b) S = 4.29 where instability growth is clearly evident.

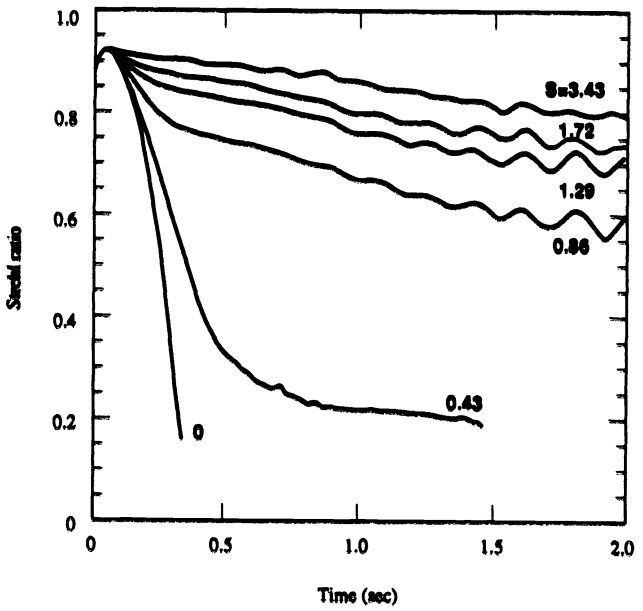

Fig. 7. Phase-compensated Strehl ratio versus time curves for a perturbation Fresnel number $N_p = 40$ and various shear values, S. All other parameters are as for Fig. 5.

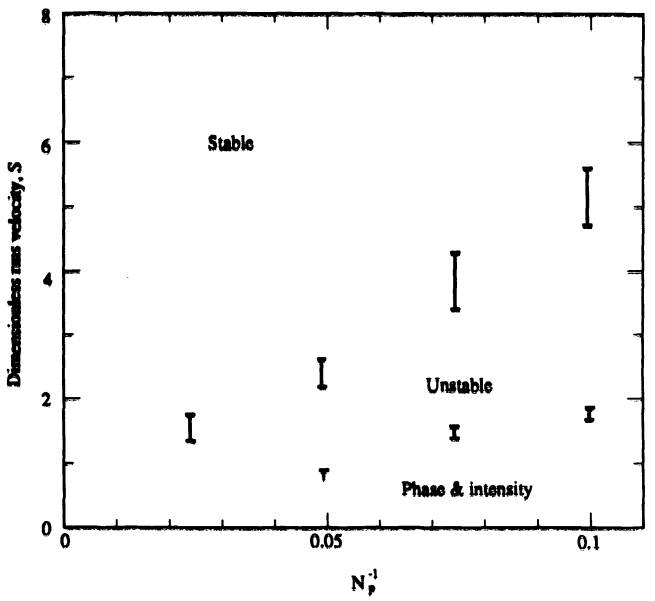

Fig. 8. The boundary between stable and unstable behavior in our calculations. The upper set of vertical bars are our results for phase-only compensation. The lower set is for phase-plus-intensity compensation in which the spatial scale of the intensity compensation was exactly matched to that of the phase compensation. In both cases the region of stable behavior lies above the bars while clearly unstable behavior occurs below the bars.